Analyst

PAPER

View Article Online
View Journal

Cite this: DOI: 10.1039/c9an02018g

Intramolecular photoinitiator induced atom transfer radical polymerization for electrochemical DNA detection†

Ligang Ma,[a] Qianrui Liu,[b] Lihe Jian,[a] Shan Ye,[a] Xiaoke Zheng*[a] and Jinming Kong *[b]

Received 10th October 2019,
Accepted 14th November 2019

DOI: 10.1039/c9an02018g

rsc.li/analyst

A novel electrochemical biosensor was reported for the first time to achieve highly sensitive DNA detection based on photoinduced atom transfer radical polymerization (photoATRP). In this work, PNA was applied as the capture probe to specifically recognize the target DNA (TDNA), and we utilized lung cancer DNA as TDNA. The ATRP initiator was introduced to the electrode surface *via* phosphate-Zr^{4+}-carboxylate chemistry. PhotoATRP was activated under blue light irradiation based on a photoinitiator I2959, which produced free radicals *via* homolytic cleavage. Subsequently, Cu^{2+} was reduced to Cu^{+} with the assistance of the free radicals, and numerous electroactive probes were grafted onto the electrode surface. Under optimal conditions, the limit of detection (LOD) of this method was 3.16 fM (S/N = 3, R^2 = 0.992), and the linear range was from 10 fM to 1.0 nM. More importantly, the preparation process of this biosensor was simple and less laborious with a low background signal, suggesting good potential in practical applications.

1. Introduction

Quantitative detection of nucleic acid is of crucial importance in many fields, including disease diagnosis, environmental monitoring and forensic analysis.[1–5] Therefore, a simple and fast method is of great importance for nucleic acid detection. Traditional detection strategies are the gold standard, such as polymerase chain reaction (PCR),[6] polyacrylamide gel electrophoresis[7] and blotting;[8] however, they are usually time consuming, high cost and complicated operation.

Atom transfer radical polymerization (ATRP) has been receiving extensive attention due to the precisely controlled molecular weight, narrow molecular weight distribution and defined architecture in various fields.[9] Recently, electrochemically mediated ATRP (eATRP) is applied for biosensing. Hu *et al*. reported a novel electrochemical DNA biosensor which was based on surface-initiated eATRP, and it achieved ultrasensitive DNA detection.[10] Subsequently, Sun and his coworkers combined eATRP and DNA-templated silver nanoparticles (AgNPs) to realize dual amplification detection of DNA.[11] Simple operation and real-time monitoring of biomolecules are the key points that need to be improved. eATRP needs more labor, the background signal is high, and it will take a long time if the samples are numerous.

Light is essential for the existence of mankind, and light-induced reactions also attract extensive attention due to the advantages of mild, affordable, easy operation and ubiquitousness.[12] Recently, photoinduced ATRP is widely applied in materials and environmental science.[13–15] However, photoATRP is rarely reported in the field of biomolecule detection.

Herein, a novel I2959-based photoATRP was reported for the first time to achieve ultrasensitive DNA detection. In this work, lung cancer DNA as target DNA (TDNA) was captured by PNA, and the photoATRP initiator (α-bromophenylacetic acid, BPAA) was linked to the electrode surface *via* phosphate-Zr^{4+}-carboxylate. PhotoATRP was activated based on I2959 and Cu^{2+} under blue light irradiation. This method showed high sensitivity, stability and specificity. More importantly, the operation of this method was simple and the detection result in human serum is also desired, indicating that this method possesses certain practical potential in the future.

2. Experimental

2.1. Materials

6-Mercapto-1-hexanol (MCH), α-bromophenylacetic acid (BPAA), 2-hydroxy-1-(4-(2-hydroxyethoxy)phenyl)-2-methyl-1-propanone (photoinitiator, I2959), dimethyl sulfoxide (DMSO)

[a]Pharmacy College, Henan University of Chinese Medicine, Zhengzhou 450008, P. R. China. E-mail: zhengxk.2006@163.com
[b]School of Environmental and Biological Engineering, Nanjing University of Science and Technology, Nanjing 210094, P. R. China. E-mail: j.kong@njust.edu.cn

†Electronic supplementary information (ESI) available. See DOI: 10.1039/c9an02018g

and tris(2-dimethylaminoethyl)amine (Me_6TREN) were all bought from Sigma-Aldrich (St Louis, MO). TE buffer (pH = 8.0), ferrocenylmethyl methacrylate (FMMA) and $LiClO_4$ were purchased from Bide Pharmatech Ltd (Shanghai, China). Potassium nitrate (KNO_3), potassium bromide (KBr), potassium hexacyanoferrate(II) ($K_4[Fe(CN)_6]$), potassium ferricyanide ($K_3[Fe(CN)_6]$), copper(II) bromide ($CuBr_2$) and human serum were acquired from Yi-Ji Co., Ltd (Shanghai, China). All reagents were of analytical grade, and ultrapure water (≥18.25 MΩ) used through the experiment was prepared from a Millipore Milli-Q water purification system.

Thiolated peptide nucleic acid (PNA), target DNA (TDNA), single base mismatched DNA (SBM), three base mismatched DNA (TBM) and control DNA (CDNA) were all purchased from Panagene Inc. (South Korea). The sequences of PNA, TDNA, SBM, TBM and CDNA are listed in Table 1, and the mismatched bases are underlined.

30% H_2O_2 and 98% H_2SO_4 (1 : 3 in volume) were used to freshly prepare piranha solution for chemically pretreating the Au electrode. TE buffer was employed to dilute PNA, TDNA, SBM, TBM and CDNA. 5.0 mM MCH (dissolved in 70% ethanol) was used to displace the non-specifically adsorbed PNA on the Au electrode surface. 5.0 mM $ZrOCl_2$ and 1.0 mM BPAA were respectively dissolved in 10% and 15% ethanol. The photoATRP cocktail was freshly prepared by adding 1 mL of 20 mM FMMA, 1 mL $CuBr_2$, 1 mL Me_6TREN, 1 mL I2959 and 1 mL DMSO into 5 mL of 0.1 kBr.

2.2 Apparatus

Cyclic voltammetry (CV) and square wave voltammetry (SWV) were performed on a CHI 660 electrochemical workstation, and a saturated calomel electrode (SCE), a Au electrode (2 mm in diameter) and a platinum wire constituted this traditional three-electrode system of the electrochemical workstation. Electrochemical impedance spectroscopy (EIS) was carried out on an Autolab/PGSTAT302N potentiostat/galvanostat (Eco Chemie, Netherlands). The light was emitted by a 470 nm blue light which consisted of 20 LEDs, and the intensity was 4.0 mW cm^{-2} (LIU470A, Thorlabs). Atomic force microscopy (AFM) was conducted on a Dimension Icon, and the scan size was 2 μm (Bruker Nano Inc., USA). The static water contact angle (WCA) was measured on a droplet shape analyzer DSA100 (KRÜSS, Germany).

2.3 Preparation of the electrochemical biosensor

The Au electrode needed to be pretreated, according to the previous literature.[16,17] After that, 5 μL of 0.5 μM PNA was dropped on the electrode surface at 37 °C for 90 min, and subsequently the electrode was washed with TE buffer. The modified electrode was immersed in 400 μL of 5 mM MCH at 37 °C for 30 min. The electrode was rinsed with 70% ethanol and ultrapure water. Afterwards, 5 μL TDNA was dropped onto the electrode surface at 37 °C for 90 min. After being washed with TE buffer, the electrode was immersed in 400 μL of 5 mM $ZrOCl_2$ at 37 °C for 15 min and washed with 10% ethanol and ultrapure water. Then, the electrode was incubated in 400 μL of 1 mM BPAA at 37 °C for 30 min and washed with 15% ethanol and ultrapure water.

The prepared electrode was immersed in the photoATRP cocktail, followed by blue light irradiation at room temperature. After the photoATRP, the electrode was respectively rinsed with DMSO and ultrapure water to remove the adsorbed monomer.

The PNA/MCH/TDNA/Zr^{4+}/BPAA/FMMA-modified electrode was detected with SWV, and the potential range of SWV was from 0 V to 0.6 V.

Table 1 The sequences of PNA, TDNA, SBM, TBM and CDNA

Name	Sequences
PNA	5′-SH-$(CH_2)_{11}$-$(Olinker)_3$-GAAGGGAGGAATGGTGTCAGGGGCG-3′
TDNA	5′-CGCCCCTGACACCATTCCTCCCTTC-3′
SBM	5′-CGCCCCTAACACCATTCCTCCCTTC-3′
TBM	5′-CGCCCATGACACTATTCCTCGCTTC-3′
CDNA	5′-TATTATCCGTCAGTGGAAAGGACCG-3′

3. Results and discussion

3.1 The mechanism of photoATRP in this DNA biosensor

The construction process of this electrochemical DNA biosensor and mechanism of photoATRP are illustrated in Scheme 1. In this biosensor, PNA was applied as the capture probe of tDNA due to the neutral backbone without phosphate. Then, the ATRP initiator (BPAA) was linked to the Au electrode surface *via* coordination of Zr^{4+} with the phosphate of TDNA and carboxylate of BPAA. Under light irradiation, photoATRP was activated.

The photoATRP can be classified into two photochemical processes.[18,19] One is the photoredox process, and the other is the intramolecular process. In this work, the intramolecular process was applied to initiate this polymerization reaction based on the photoinitiator I2959. Under light irradiation, an electron of the ground state of I2959 was excited from the highest occupied molecular orbital (HOMO) into a higher lying orbital *via* absorbing a photon. In the light of Kasha's rule, no matter which higher lying orbital was occupied, a single excited state of I2959 would be generated due to the fast thermal relaxation. The single excited state of I2959 would produce two free radicals (R$^\bullet$, benzoyl and α-substituted alkyl radicals) *via* homolytic cleavage.[20] The R$^\bullet$ could readily reduce Cu^{2+} Br/L to Cu^+/L, and photoATRP was activated (L is the ligand of the copper atom). In the initiation of polymerization, Cu^+/L snatched the bromine atom of the ATRP initiator (BPAA), while Cu^{2+} Br/L and a primary radical ($P_0^\bullet$) were generated. The regenerated Cu^{2+}Br/L was again reduced to Cu^+/L. At the same time, $P_0^\bullet$ attacked the carbon–carbon double bond of methyl methacrylate contained in FMMA, and the polymer chain continuously grew.

In this intramolecular process, it is noted that benzoyl and α-substituted alkyl radicals produced by I2959 might attack the ATRP monomer. However, the formed $R_n^\bullet$ could also reduce

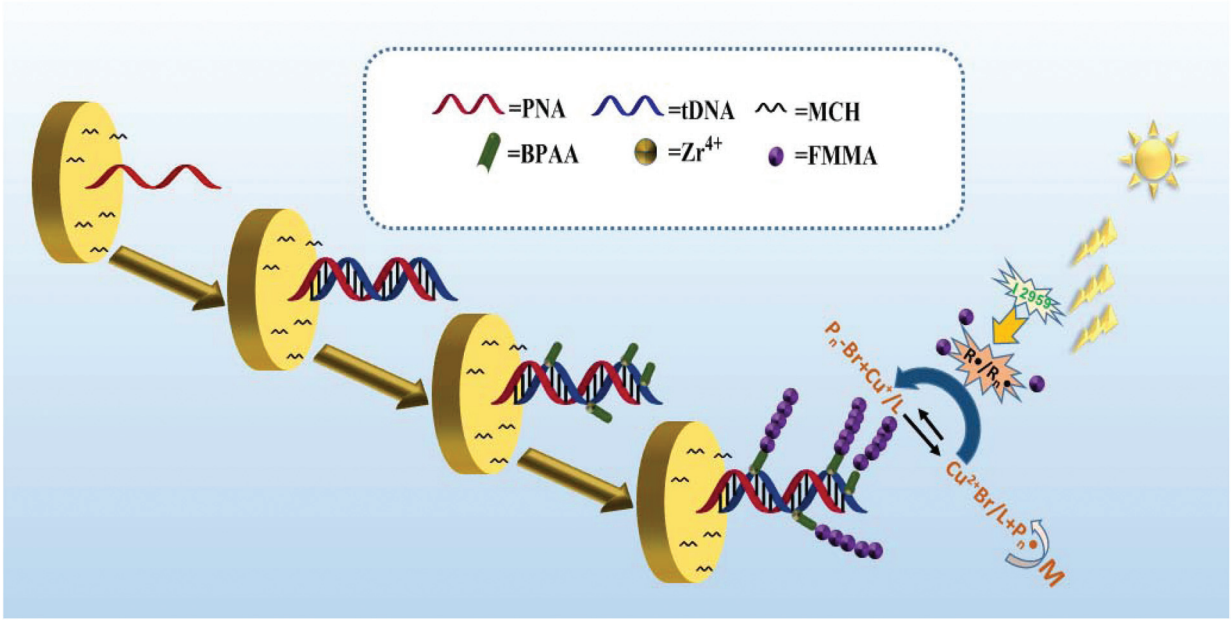

Scheme 1 The illustration of electrochemical DNA biosensor construction and mechanism of photoATRP.

the Cu^{2+} Br/L to Cu^{+}/L. The excessive free radicals would promote the polymerization.[20]

3.2 Characterization of the electrode surface

Atomic force microscopy (AFM) analysis was applied to visualize the electrode surface and quantitatively measure the surface height and roughness (R_a) before and after the photoATRP on the gold chip. As shown in Fig. 1A, the surface height and R_a of the PNA/MCH/tDNA/Zr^{4+}/BPAA-modified gold chip were respectively 27.6 nM and 2.97 nM. After the photoATRP, the surface height and R_a respectively increased to 35.1 nM and 3.91 nM (Fig. 1B). The increased surface height and R_a indicated that photoATRP successfully occurred on the gold chip, and the material on the surface of the gold chip became dense after photoATRP which suggested the formation of polymeric chains.

The water contact angle (WCA) was measured to investigate the hydrophilicity and hydrophobicity of the modified material on the gold electrode surface. If the material is hydrophobic, the angle is more than 90°; if the angle is less than 90°, the material is hydrophilic. The better the hydrophilicity of the material, the smaller the water contact angle. As shown in Fig. S1,† the angle of the bare electrode was 99.3° due to the hydrophobicity of the Au electrode (Fig, S1a†). After PNA was immobilized on the electrode surface, the angle decreased to 65.3° (Fig. S1b†). The hydrophilic group (hydroxyl) of MCH led

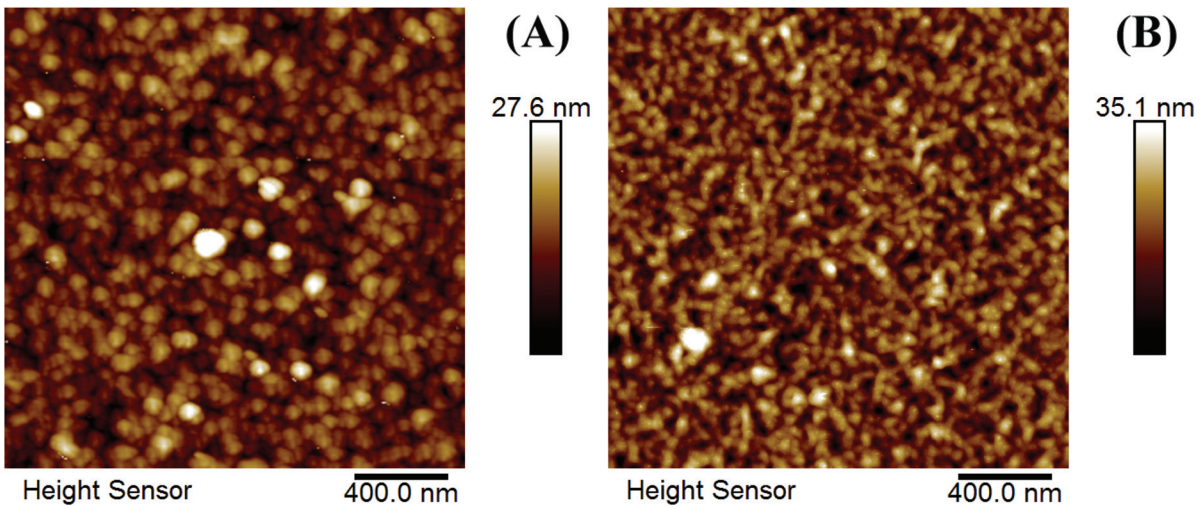

Fig. 1 AFM 2D images of PNA/MCH/TDNA/Zr^{4+}/BPAA-modified (A) and PNA/MCH/TDNA/Zr^{4+}/BPAA/FMMA-modified gold chips.

to the decrease of angle (54.6°, Fig. S1c†). The angle further decreased (50.9°, Fig. S1d†) after TDNA was added to the electrode surface. This result was because the backbone of TDNA contained a hydrophilic group (phosphate), and this result also demonstrated the successful hybridization between PNA and tDNA. The angle increased (61.1°, Fig. S1e†) after Zr^{4+} was linked to the electrode surface. This result was ascribed to the coordination between Zr^{4+} and phosphate which resulted in the deterioration of hydrophilicity. The hydrophobic group (phenyl) caused the further deterioration of hydrophilicity after BPAA was attached to the electrode surface (66.8°, Fig. S1f†). After photoATRP, numerous FMMA were introduced to the electrode surface and the angle decreased (57.9°, Fig. S1g†) which was because methyl methacrylate is more hydrophilic than phenyl. This result also suggested that the photoATRP was successful on the electrode surface.

3.3 Electrochemical characterization of the biosensor

SWV was applied to assess the feasibility of this electrochemical DNA biosensor on the basis of control experiments in 1.0 M $LiClO_4$, and the potential range was from 0 V to 0.6 V. As shown in Fig. 2A, if all reagents were present, an apparent oxidation was observed at a potential of 0.3 V, and this potential value was in the oxidation potential range of ferrocene (Fig. 2A, a). No obvious peak was observed if PNA was absent from the biosensor which was because TDNA was not recognized by PNA and the ATRP initiator was disabled to introduce to the electrode surface, indicating that PNA was used as the capture probe of TDNA which was the primary premise of this biosensor (Fig. 2A, b). Likewise, if TDNA was not added to the biosensor, no peak was seen which was observed from the curve c of Fig. 2A. If BPAA was not present in this biosensor, no peak was observed (Fig. 2A, d). This result was because the ATRP initiator was indispensable to photoATRP. If Cu^{2+} was absent, no peak was seen (Fig. 2A, e); especially, the radicals produced by I2959 might also attack the ATRP monomer. However, the polymer chains formed in the photoATRP cocktail were independent of the electrochemical detection signal. It is worth noting that a weak peak was observed when I2959 was absent from the biosensor (Fig. 2A, f). This result was presumably because less Cu^{+}/L was produced from Cu^{2+}Br/L under blue light irradiation.[14,21] No peak was seen if light was absent, indicating that the light was essential for polymerization (Fig. 2A, g). A series of control experiments demonstrated that this method was feasible.

CV was applied to characterize the modification method of FMMA at different scan rates in 1.0 $LiClO_4$, and the potential range was from 0 V to 0.6 V. As shown in Fig. 2B, the anode and cathode current respectively presented a good linear relationship with different scan rates (10 mV s^{-1}, 25 mV s^{-1}, 50 mV s^{-1}, 75 mV s^{-1}, 100 mV s^{-1}, 150 mV s^{-1}, 250 mV s^{-1}, 500 mV s^{-1}, 750 mV s^{-1}, and 1000 mV s^{-1}). This result suggested that FMMA was immobilized on the electrode *via* a strong force rather than adsorption and this redox was a surface controlled process not a diffusion process.

EIS was usually used to monitor the construction process of this electrochemical biosensor *via* a novel strategy in 5.0 mM $[Fe(CN)_6]^{3-/4-}$ in 0.1 M KNO_3, and the frequency range was from 0.1 Hz to 100 kHz. The diameter of the semicircle represents the charge transfer resistance (R_{ct}) in Nyquist plots. As shown in Fig. 2C, the bare electrode showed a smallest R_{ct} due to the fast charge transfer between the electrode surface and the solution (~190 Ω, Fig. 2Ca). After PNA was immobilized onto the electrode surface, the R_{ct} increased to ~231 Ω which was because a self-assembled molecular layer of PNA hindered the charge transfer to a certain extent (Fig. 2Cb). The R_{ct} further increased after MCH was added onto the surface due to the denser self-assembled molecular layer (~579 Ω, Fig. 2Cc). These results suggested that PNA and MCH were successfully immobilized onto the electrode surface *via* Au–S bonds. After TDNA was added into the electrode surface, R_{ct} increased to ~951 Ω due to the repulsion caused by the negative charge of the phosphate backbone of TDNA and $[Fe(CN)_6]^{3-/4-}$, indicating successful formation of PNA/DNA heteroduplexes (Fig. 2Cd). When Zr^{4+} was added into this biosensor, R_{ct} continuously increased (~1725 Ω, Fig. 2Ce). This

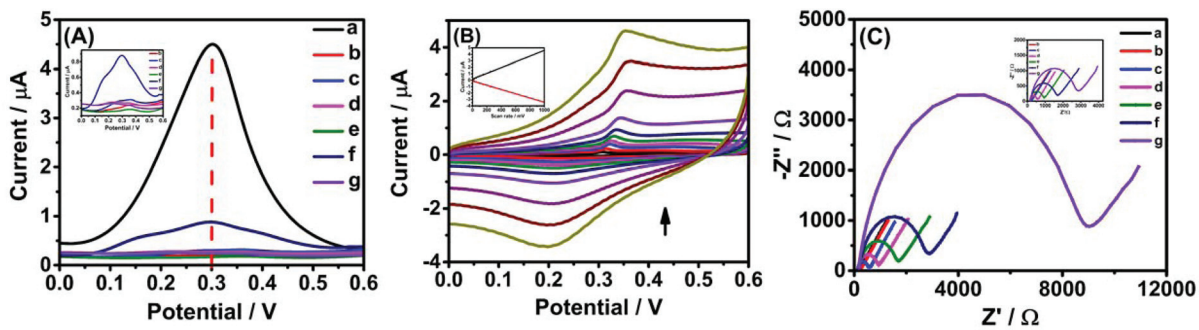

Fig. 2 (A) The SWVs of the PNA/MCH/TDNA/Zr^{4+}/BPAA/FMMA-modified electrode (a) and in the absence of PNA (b), TDNA (c), BPAA (d), Cu^{2+} (e), I2959 (f) or light (g). Inset: the SWVs of b–g. (B) CVs of FMMA on the electrode surface at different scan rates in 1.0 M $LiClO_4$ (10 mV s^{-1}, 25 mV s^{-1}, 50 mV s^{-1}, 75 mV s^{-1}, 100 mV s^{-1}, 150 mV s^{-1}, 250 mV s^{-1}, 500 mV s^{-1}, 750 mV s^{-1}, and 1000 mV s^{-1}). Inset: the linear relationship between oxidation currents and reduction currents and scan rates. (C) The EIS of the bare electrode (a), PNA-modified electrode (b), PNA/MCH-modified electrode (c), PNA/MCH/TDNA-modified electrode (d), PNA/MCH/TDNA/Zr^{4+}-modified electrode (e), PNA/MCH/TDNA/Zr^{4+}/BPAA-modified electrode (f), and PNA/MCH/TDNA/Zr^{4+}/BPAA/FMMA-modified electrode (g). Inset: the SWVs of a–f.

result might be because the electrostatic attraction between Zr^{4+} and $[Fe(CN)_6]^{3-/4-}$ led to the attachment of $[Fe(CN)_6]^{3-/4-}$ to PNA/DNA heteroduplexes, and previously attached $[Fe(CN)_6]^{3-/4-}$ and the $[Fe(CN)_6]^{3-/4-}$ in solution would generate electrostatic repulsion which caused the increase of R_{ct}. After the ATRP initiator was added into the electrode surface, R_{ct} increased to ~2884 Ω (Fig. 2Cf). The R_{ct} dramatically increased after photoATRP, indicating that photoATRP was successful on the electrode surface (~9176 Ω, Fig. 2Cg). Moreover, these results also implied the successful construction process of this biosensor.

3.4 Optimization of conditions

To achieve the best analytical performance, the condition optimization of photoATRP based on I2959 is necessary for this analytical method. Firstly, the amount of I2959 was optimized. As shown in Fig. 3A, the current signal increased with the increase of I2959 concentration before 0.2 mM I2959 due to the increase of R• (benzoyl and α-substituted alkyl radicals) produced by I2959. After that, the current decreased. This was because the superabundant R•(benzoyl and α-substituted alkyl radicals) disturbed the photoATRP on the electrode surface. Thus, 0.2 mM was used as the optimal concentration of I2959.

As shown in Fig. 3B, the current rapidly increased with the increase of Cu^{2+} before 0.1 mM Cu^{2+}, followed by a slow increase of current. 0.1 mM was selected as the optimal concentration of Cu^{2+}. The light time was an essential condition of this analytical method. As shown in Fig. 3C, the current signal increased with the increase of light time. 2 h was used as the optimal time in this method.

3.5 The analytical performance

SWV was applied to assess the analytical performance of this biosensor in 1.0 $LiClO_4$, and the potential was from 0 V to 0.6 V. Under optimal conditions, different concentrations of TDNA were detected from 1 nM to 0.01 pM. As shown in Fig. 4A, the oxidation current of FMMA increased with the increase of TDNA concentrations. From the calibration plots in Fig. 4B, the logarithm of different TDNA concentrations and the current signal showed a good linear relationship, and the

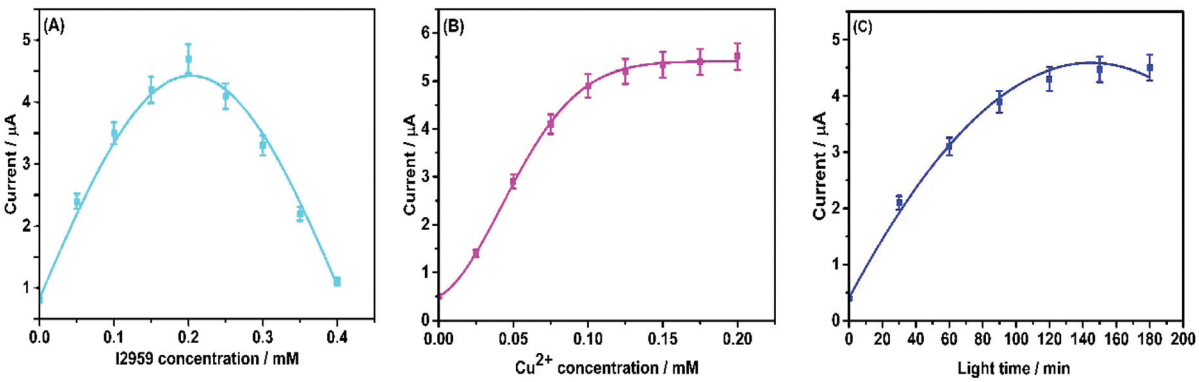

Fig. 3 Effects of the I2959 concentration (A), the Cu^{2+} concentration (B), and the light time (C) on the analytical performance of this method in 1.0 M $LiClO_4$.

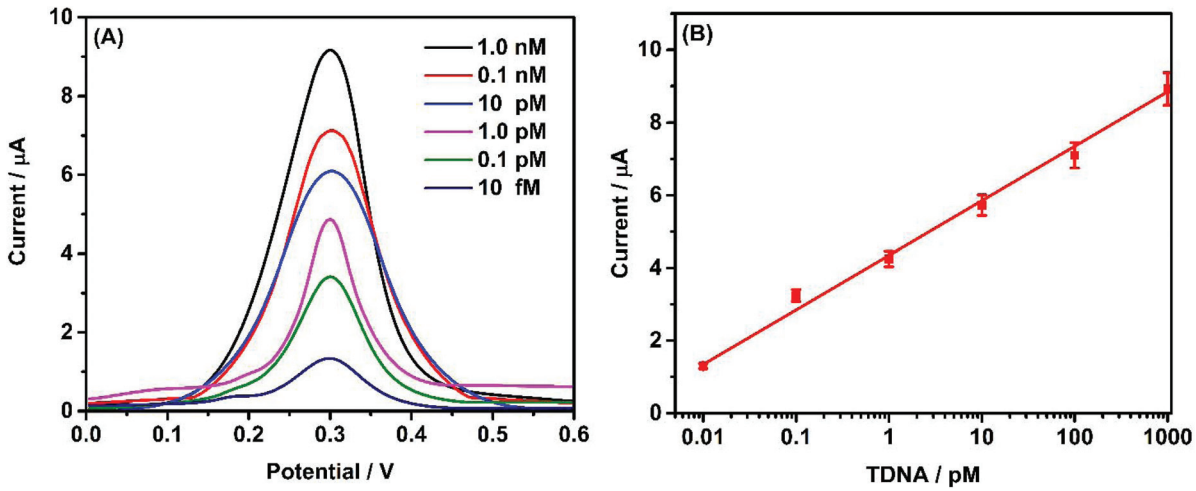

Fig. 4 (A) SWVs of the prepared electrodes towards different TDNA concentrations (1.0 nM, 0.1 nM, 10 pM, 1.0 pM, 0.1 pM, and 10 fM). (B) The calibration plots between the current of FMMA and the logarithm of TDNA concentrations.

Table 2 Comparison of this strategy with other strategies for ultrasensitive DNA detection

Method	Linear range	LOD	Ref.
Fluorescence	2 nM to 150 nM	1.6 nM	22
Fluorescence	0.5 nM to 50 nM	0.20 nM	23
Fluorescence	0.1 nM to 10 nM	98.2 pM	24
Fluorescence	0 to 100 fM	50 fM	25
Electrochemistry	100 nM to 10 fM	10 fM	26
PCR	16 fM to 1.6 nM	4.3 fM	27
Electrochemistry	10 fM to 1.0 nM.	3.16 fM	This work

linear regression equation was I (μA) = 1.502 log[TDNA/pM] + 4.346 (R^2 = 0.992) with a linear range from 10 fM to 1.0 nM. The LOD was calculated to be 3.16 fM (S/N = 3). As summarized in Table 2, the LOD of this method was lower than that of many other methods. This was because polymerization would introduce numerous electroactive probes which led to the dramatic improvement of sensitivity. The operation of this method was very easy and environment friendly to some extent.

3.6 The stability and repeatability of the biosensor

The prepared electrodes, that is, PNA/MCH/TDNA/Zr^{4+}/BPAA/FMMA-modified electrodes, were stored at 4 °C and the moisture was saturated.[28] The storage time was about two weeks. The recovery of the current signal was 91.4%. This result indicated that the stability of this biosensor was satisfactory.

Six intra-assays and inter-assays were respectively conducted to evaluate the repeatability of this biosensor. The RSD was respectively 3.6% and 4.9%. This result suggested that the repeatability of this method was appropriate.

3.7 Specificity and practical application

The specificity of this biosensor was assessed *via* applying SWV to detect SBM, TBM and CDNA, and the potential range of SWV was from 0 V to 0.6 V in $LiClO_4$.[29,30] The concentrations of all those DNA were 1.0 pM. The current signal of TDNA was compared with that of SBM, TBM and CDNA, under the same experimental conditions. As shown in Fig. 5A, the recoveries of SBM and TBM were respectively 33.7% and 19.7%, while the current signal of CDNA was close to the background signal. These results were because the mismatched bases caused unfavorable hybridization between PNA and DNA due to the high specificity of PNA. Therefore, the number of phosphates of DNA decreased which directly led to the reduction of the ATRP initiator, and the final current signal dramatically decreased. These results indicated that this photoATRP guaranteed a desired specificity of this biosensor.

10% normal human serum (NHS) was utilized to simulate the human environment for evaluating the practical application of this method.[31,32] The TDNA was diluted to 1.0 pM, 0.1 pM and 0.01 pM with 10% NHS, and the current signal was respectively compared with that of 1 pM TDNA, 0.1 pM TDNA and 0.01 pM TDNA diluted with TE buffer. As shown in Fig. 5B, the recovery of the current signal was 96.4%, 95.6%, and 94.1%. This result demonstrated that this method showed a satisfactory practical application.

4. Conclusions

To sum up, a novel electrochemical DNA biosensor was reported *via* I2959-based photoATRP. Free radicals were produced *via* homolytic cleavage of I2959 with the help of light, and the free radicals reduced Cu^{2+} to Cu^{+}. PhotoATRP was started to graft numerous electroactive probes onto the electrode surface. The LOD of this method was 3.16 fM (R^2 = 0.992), and thus this method achieved high sensitivity for lung cancer DNA. The specificity and stability of this method were both satisfactory, and the detection result in normal human serum was also desired. Different DNA sequences can be detected *via* designing PNA sequences, and this strategy might be activated under sunlight. Therefore, this photoATRP showed significant potential in the field of biomolecule detection.

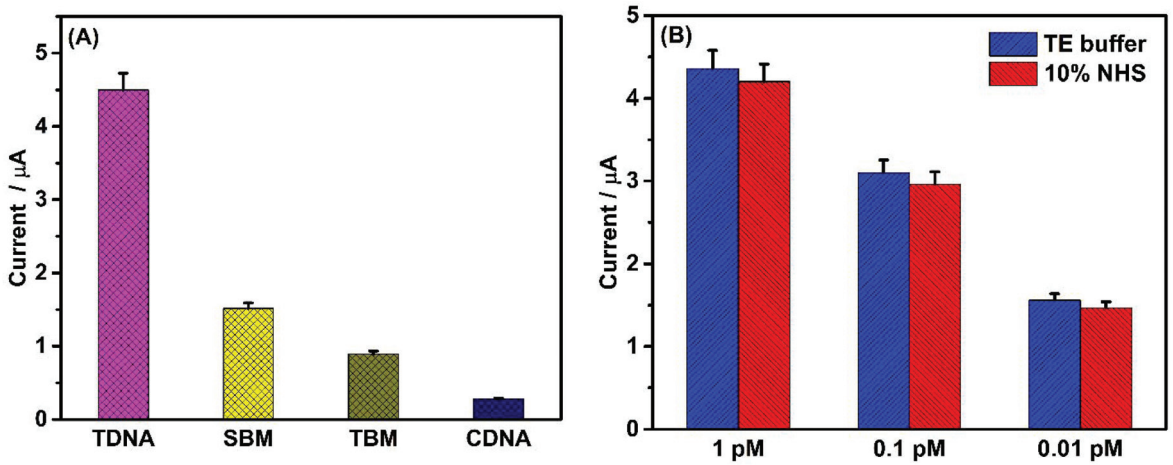

Fig. 5 (A) SWV response of 1.0 pM TDNA, 1.0 pM SBM, 1.0 pM TBM and 1.0 pM CDNA. (B) SWV response of 1.0 pM, 0.1 pM and 0.01 pM in TE buffer and 10% NHS.

Conflicts of interest

There are no conflicts to declare.

Acknowledgements

The authors thank the National Key Research and Development Project (The Major Project16 for Research of the Modernization of TCM): Key Technology Research for the Characteristic Chinese Medicine Industry Chain of Rehmannia glutinosa (2017YFC1702800); the Major Science and Technology Projects in Henan Province: Study on the key technology for quality control and the key characteristics of Rehmannia glutinosa, Dioscorea opposita Thunb and Achyranthes bidentata Blume from Henan Province (171100310500); and the National Natural Science Foundation of China (21974068).

References

1 Y. Song, X. Yan, G. Ostermeyer, S. Q. Li, L. B. Qu, D. Du, Z. H. Li and Y. H. Lin, *Anal. Chem.*, 2018, **90**, 10369–10376.
2 T. Hou, W. Li, X. J. Liu and F. Li, *Anal. Chem.*, 2015, **87**, 11368–11374.
3 C. H. Fan, K. W. Plaxco and A. J. Heeger, *Proc. Natl. Acad. Sci. U. S. A.*, 2003, **100**, 9134–9137.
4 Y. Wang, Z. H. Li, M. S. Liu, J. J. Xu, D. H. Hu, Y. H. Lin and J. H. Li, *Anal. Chim. Acta*, 2017, **983**, 1–8.
5 P. P. Gai, C. C. Gu, H. Y. Li, X. Z. Sun and F. Li, *Anal. Chem.*, 2017, **89**(22), 12293–12298.
6 W. T. Xua, N. Cheng, K. L. Huang, Y. H. Lin, C. G. Wang, Y. C. Xu, L. J. Zhu, D. Du and Y. B. Luo, *Biosens. Bioelectron.*, 2016, **80**, 654–660.
7 X. L. Zhu, H. Shi, Y. L. Shen, B. Zhang, J. Zhao and G. X. Li, *Nano Res.*, 2015, **8**, 2714–2720.
8 S. M. Harding, J. L. Benci, J. Irianto, D. E. Discher, A. J. Minn and R. A. Greenberg, *Nature*, 2017, **548**, 466–470.
9 J. C. Theriot, C. H. Lim, H. S. Yang, M. D. Ryan, C. B. Musgrave and G. M. Miyake, *Science*, 2016, **352**, 1082–1086.
10 Q. Hu, Q. W. Wang, G. Z. Sun, J. M. Kong and X. J. Zhang, *Anal. Chem.*, 2017, **89**, 9253–9259.
11 H. B. Sun, J. M. Kong, Q. W. Wang, Q. R. Liu and X. J. Zhang, *ACS Appl. Mater. Interfaces*, 2019, **11**, 27568–27573.
12 D. Ravelli and M. Fagnoni, *ChemCatChem*, 2012, **4**, 169–171.
13 D. Konkolewicz, K. Schröder, J. Buback, S. Bernhard and K. Matyjaszewski, *ACS Macro Lett.*, 2012, **1**, 1219–1223.
14 M. A. Tasdelen, M. Uygun and Y. Yagci, *Macromol. Chem. Phys.*, 2011, **212**, 2036–2042.
15 E. Murtezi and Y. Yagci, *Macromol. Rapid. Commun.*, 2014, **35**, 1782–1787.
16 Q. Hu, X. B. Deng, J. M. Kong, Y. Y. Dong, Q. R. Liu and X. J. Zhang, *Analyst*, 2015, **140**, 4154–4161.
17 Q. Hu, J. M. Kong, D. X. Han, L. Niu and X. J. Zhang, *ACS Sens.*, 2019, **4**, 235–241.
18 N. Corrigan, J. Yeow, P. Judzewitsch, J. T. Xu and C. Boyer, *Angew. Chem.*, 2019, **131**, 5224–5243.
19 M. Chen, M. J. Zhong and J. A. Johnson, *Chem. Rev.*, 2016, **116**, 10167–10211.
20 M. Ciftci, M. A. Tasdelen, W. W. Li, K. Matyjaszewsk and Y. Yagci, *Macromolecules*, 2013, **46**, 9537–9543.
21 A. Anastasaki, V. Nikolaou, Q. Zhang, J. Burns, S. R. Samanta, C. Waldron, A. J. Haddleton, R. McHale, D. Fox, V. Percec, P. Wilson and D. M. Haddleton, *J. Am. Chem. Soc.*, 2014, **136**, 1141–1149.
22 W. Ding, C. Song, T. L. Li, H. R. Ma, Y. W. Yao and C. Yao, *Talanta*, 2019, **199**, 442–448.
23 F. Tao, J. Fang, Y. C. Guo, Y. Y. Tao, X. L. Han, Y. X. Hu, J. J. Wang, L. Y. Li, Y. L. Jian and G. M. Xie, *Anal. Biochem.*, 2018, **554**, 16–22.
24 W. W. Hu, Y. Ning, J. M. Kong and X. J. Zhang, *Analyst*, 2015, **140**, 5678–5684.
25 I. A. Iwe, Z. G. Li and J. H. Huang, *Analyst*, 2019, **144**, 2649–2655.
26 M. Chen, Y. Y. Wang, H. L. Su, L. Mao, X. N. Jiang, T. Zhang and X. Z. Dai, *Sens. Actuators, B*, 2018, **255**, 2910–2918.
27 L. Zou, R. D. Shen, L. S. Ling and G. K. Li, *Anal. Chim. Acta*, 2018, **1038**, 105–111.
28 Q. Hu, X. B. Deng, X. H. Yu, J. M. Kong and X. J. Zhang, *Biosens. Bioelectron.*, 2015, **65**, 71–77.
29 H. B. Sun, W. Xu, B. Liu, Q. R. Liu, Q. W. Wang, L. Z. Li, J. M. Kong and X. J. Zhang, *Anal. Chem.*, 2019, **91**, 9198–9205.
30 C. X. Song, B. J. Li, X. H. Yang, K. M. Wang, Q. Wang, J. B. Liu and J. Huang, *Analyst*, 2017, **142**, 224–228.
31 S. Takalkar, K. Baryeh and G. D. Liu, *Biosens. Bioelectron.*, 2017, **98**, 147–154.
32 S. F. Liu, C. B. Cheng, T. Liu, L. Wang, H. W. Gong and F. Li, *Biosens. Bioelectron.*, 2015, **63**, 99–104.